Composites: Part A 187 (2024) 108510

Contents lists available at ScienceDirect

Composites Part A

journal homepage: www.elsevier.com/locate/compositesa

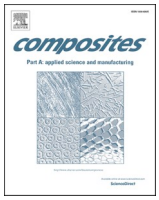

Design of experiments investigation into the production of all cellulose composites using regenerated cellulosic textiles

Ashley Victoria [a], Peter John Hine [a], Keeran Ward [b], Michael Edward Ries [a,*]

[a] School of Physics and Astronomy, University of Leeds, Woodhouse Lane, Leeds LS2 9JT, UK
[b] School of Chemical and Process Engineering, University of Leeds, Woodhouse Lane, Leeds LS2 9JT, UK

ARTICLE INFO

Keywords:
A.Materials: Cellulose
Biocomposite
Fabrics/textiles
C.Analysis: Statistical properties/methods

ABSTRACT

All cellulose composites (ACCs) can be produced from native and man-made cellulosic fibres; use of the latter provides an additional application for waste-derived regenerated fibers. ACCs were prepared using an ionic liquid dissolution method, utilizing a regenerated cellulose (Tencel) textile, with and without an interleaf cellulosic film. A design of experiments methodology was applied to explore process-property relationships; concentration of the ionic liquid and the processing time and temperature were investigated. It was found that the film remained in-between the textile layers, rather than penetrating the fiber assembly, in contrast to our previous work on cotton-based ACCs. This is due to the structural differences between Tencel and cotton fabric. A multi-response optimization was conducted through a central composite face centered strategy, which captured the film system more strongly. Optimized processing conditions were identified, yielding a Young's modulus and strain-to-failure of 5.3 GPa and 3.5% respectively, validated through in-lab samples.

1. Introduction

In recent years, all-cellulose composites (ACCs) have been a topic of growing interest in addressing the need to develop renewable material alternatives to traditional fossil fuel derived composites [1–9]. In contrast to traditional composite materials, whereby the matrix and reinforcing components are formed from different materials, ACCs feature matrix and reinforcing components comprising entirely of cellulose [4,10–12]. Cellulose is a renewable biopolymer found in nature [1,2,13], possessing intrinsically good mechanical properties [14]. With increasing concerns over resource scarcity and climate change [8,15], utilising renewable biomass is becoming a crucial focus to support the development of sustainable materials. The one-component system offered by ACCs additionally overcomes the challenges faced in recycling processes, where separation of mixed components would be required [1,8,16].

Cellulosic fibres can be produced via chemical means to produce man-made cellulosic fibres (MMCFs) [17]. Global production of MMCFs has more than doubled over the last 20 years from 3 million tonnes to 7.2 million tonnes, accounting for 6 % of total global fibre consumption [18]. Whilst this is comparatively small when considering the market share of cotton fibres, it is worth noting that cotton fibre production has seen a decrease since 2019. Considered a more sustainable alternative to cotton and synthetic fibres such as polyester [19], it is no surprise that production of MMCFs has grown and is expected to continue to do so [18]. Over the years, alternate routes to producing MMCFs have been developed including the Lyocell process where fibres are produced via direct dissolution of wood pulp in N-Methylmorpholine N-oxide (NMMO), eliminating the need for derivatisation as required by the viscose process [20]. Since commercialisation in 1990, lyocell fibres have gained popularity as an alternative MMCF, with a growth rate predicted to exceed that of viscose in the near future [21].

It is evident that the demand for textile fibres continues to rise, however, with increased consumption comes the potential for increased future waste accumulation, to which the textile industry is a large contributor. In 2017, over 700 thousand tonnes of household residual waste heading to landfill or incineration came from textile products, and of this, 336 thousand tonnes were clothing products [22]. At present, MMCFs are produced from wood pulp as the raw material feedstock, however there is potential to use alternative biomass feedstocks such as waste textiles, an area of which there is growing interest [23]. This reduces the demand for virgin feedstocks and offers a less destructive route to mechanical processing of textile waste that can result in low quality fibres unsuitable for textile products [24–26]. Exploring alternative

* Corresponding author.
E-mail addresses: bgy2mve@leeds.ac.uk (A. Victoria), P.J.Hine@leeds.ac.uk (P.J. Hine), K.Ward@leeds.ac.uk (K. Ward), m.e.ries@leeds.ac.uk (M.E. Ries).

https://doi.org/10.1016/j.compositesa.2024.108510
Received 12 July 2024; Received in revised form 11 September 2024; Accepted 5 October 2024
Available online 6 October 2024

ways to valorise textile waste is a worthwhile area of investigation [27,28] and in the context of ACCs, the use of post-consumer textiles is garnering interest [1,29,30].

The utilization of textile waste to produce cellulosic fibres is an active area of research [25,26,31,32], and its potential to overcome these barriers is clear, producing a homogenous fibre that can be woven into a textile preform for use in ACCs. Additionally, this creates a fully circular system whereby the ACC can be re-dissolved after use, re-spun into fibres to be woven into textile, and the process started again. To realise the potential of such technology, further process understanding is required to obtain the best properties from regenerated cellulose-based ACCs and how they compare to the native cellulose fibres such as cotton and flax. In our previously reported work [33] we explored the use of natural cotton fibre based textiles in combination with cellulosic films to produce ACCs with enhanced interlayer adhesion [34]. A cellulose film was introduced in between the layers of cotton textile prior to dissolution in a combination of ionic liquid 1-ethyl-3-methylimidazoliam acetate ([C2MIM][OAc]), and dimethyl sulfoxide (DMSO). This was found to significantly improve the interlaminar bonding of ACCs and increase Young's modulus when compared to ACCs produced without the film. In this work we apply DoE to investigate how dissolution conditions affect the mechanical properties of ACCs produced using MMCF based textiles, namely Tencel, a fabric comprising Tencel fibres produced via the lyocell process by Lenzing AG. Additionally, the use of the interleaved cellulosic film [33] is investigated to assess its potential benefits in a predominantly cellulose II system.

DoE provides an efficient route to process understanding where several factors can be explored simultaneously, reducing the number of experimental runs needed [35–38]. Traditional one-factor-at-a-time (OFAT) methods involve varying one factor whilst keeping the others fixed [35,39,40]. Whilst this can be useful for systems with a small number of factors, it does not provide enough information about all possible factor combinations, and a more optimised region for the system may be missed. A 2^3 full factorial design was applied in the first instance to explore dissolution temperature, percentage [C2MIM][OAc] in DMSO (IL%), and dissolution time to investigate their effects on ACC mechanical properties. The experimental runs cover all combinations of the upper and lower levels of each independent factor [37,39,41], offering early insight into the appropriateness of the design space and the quality of outputs obtained at extreme process conditions, making them an ideal choice for initial screening [37]. Six additional runs at the center points were made to offer some insight into the repeatability of the process and provide a reasonable estimation of error [39,41].

The full factorial design was subsequently expanded to a response surface design to gain further insight into the process and optimise the response variable. Face-centred central composite (CCF) designs are a type of response surface design that are made up of factorial points, centre points, and star points, meaning they can build on existing factorial designs and allow quadratic effects to be estimated. The original full factorial runs are preserved in the design, and only a small number of additional runs are needed to expand this, that typically equal the number of factors multiplied by two [37,42], making it an efficient way to move from screening to optimisation.

2. Materials and methods

2.1. Materials

Regenerated cellulose (Tencel) was used for this work, purchased from Ecological Textiles, Netherlands. The fabric has an areal density of 140 g/m^2 and a thread count of 144. Natureflex 23NP cellulose film with a thickness of 23 μm was used as the interleaf cellulosic film layer, supplied by The Futamura Group. The films were used as supplied, as the small additives present in these films do not significantly affect the dissolution process [33,43]. Ionic liquid [C2MIM][OAc] with a purity of $\geq$ 95 % was purchased from ProIonic and co-solvent dimethyl sulfoxide (DMSO), with a purity of $\geq$ 99.9 %, was purchased from Fisher Scientific.

2.2. ACC processing

ACCs were produced via our previously reported method of partial dissolution with applied heat and pressure [33,43], using two layers of Tencel textile. A schematic of the process is shown in Fig. 1. In this work, the two systems under investigation; processing ACCs with two layers of textile only, and processing with the addition of the interleaved cellulosic film between the layers, are referred to as F0 and F1 respectively. Two Tencel textile layers were stacked aligning the warp yarns at 0°, giving a stacking sequence of (0,0). The stack was then immersed in a solution of [C2MIM][OAc] and DMSO, and subsequently placed in a laboratory heat press and heated under pressure. A fixed processing pressure of 2.3 MPa was used for all the experiments. Pressure was explored through DoE in our previous work on cotton-based ACCs [43], where it was found to have no significant effect on the resulting ACC properties. A setting of 2.3 MPa does, however, allow the textile stack to maintain shape during processing. The textile layers were weighed to determine the dry mass of cellulose to be processed, and a solvent to cellulose (S/C) weight ratio of 3:1 was used. This aligns with our previous work where it was found that a 3:1 S/C weight ratio resulted in sufficient matrix production to yield a fully consolidated ACC [33]. This helps to overcome flashing, where excess dissolved cellulose is expelled from the stack when pressure is applied. Additionally, there is no gain from limiting solvent use at laboratory scale when scaling up would involve the use of a solvent bath, exposing the textile substrate to excess solvent. The solvent solution comprised a mixture of [C2MIM][OAc] and DMSO, with the % by weight of [C2MIM][OAc] being one of the process factors studied. In our previous work using cotton textiles, the % weight of [C2MIM][OAc] was explored through the one-factor-at-a-time (OFAT) method, where it was found that adding 20 % DMSO allows for ease of application to the textile stack by lowering the viscosity of [C2MIM][OAc][33]. In this work, the % by weight of [C2MIM][OAc] was varied from 30 % to 100 % to explore its influence further. Dissolution time and temperature were also varied as part of the experimental design. After dissolution, the samples were placed in a coagulation bath of distilled water at room temperature and left for 1200 min (20 h) to allow the solvent to be removed. The stack was then dried in the heat press at fixed temperature, pressure, and time of 125 °C, 2.3 MPa and 60 min respectively [33,34,43].

2.3. Mechanical testing

Tensile strength, Young's modulus and strain-to-failure were evaluated using an Instron 5584 universal tensile tester according to ASTM D1846. Test specimens were cut using a laser cutter to a gauge length of 30 mm and width of 5 mm and tested using a crosshead speed of 10 mm/min.

2.4. Materials Characterisation

2.4.1. Density measurement

A gravimetric approach was used to determine the densities of the optimized ACCs. The dimensions of cut specimen samples were measured using an RS PRO digital caliper to obtain the specimen volume, and subsequently weighed. For each ACC, three specimens were measured and weighed to obtain an estimation of error. A reference value of 1.5 g/cm^3 was used for the density of the cellulosic materials within the ACC, drawing from existing literature. The density of plant fibers is reported to be between 1.4 and 1.5 g/cm^3 [44], cellulose II is reported to have an approximate density at 1.5 g/cm^3, and the density of bulk amorphous cellulose is estimated to be in the range of 1.48 to 1.5 g/cm^3 [45].

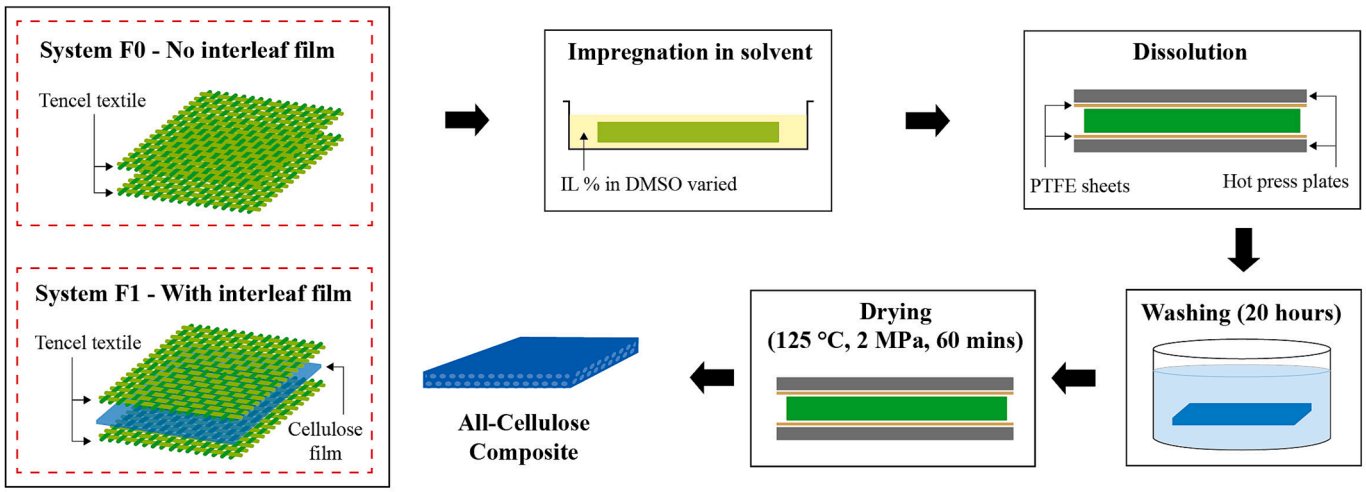

Fig. 1. Schematic of the stages involved in the preparation and manufacture of the ACCs.

2.4.2. Optical microscopy

Cross-sections of the prepared ACCs were observed using an Olympus BH2 microscope in reflection mode. Composite thickness measurements were then extracted from these images utilizing ImageJ software. To enhance image clarity, samples were embedded in epoxy resin using a silicon mold and subsequently polished. To ensure an accurate representation of each sample was presented in this paper, multiple images were obtained from which thickness measurements were taken. For each ACC sample, an average thickness value, along with the corresponding standard error, was calculated from six measurements.

2.5. Experimental design

2.5.1. Full factorial design

A 2^3 full factorial design was used for preliminary exploration of compaction temperature, process time, and % by weight of [C2MIM][OAc] (IL %), and their influence on ACC properties. Here, the three continuous, independent factors each have 2 levels that represent the minimum and maximum settings. Fig. 2 outlines the experimental domain within which the experiments would be performed as determined through preliminary screening experiments and insights from previous work [43], allowing the experimental domain to be refined for the full factorial design. The final minimum and maximum settings were ascertained to ensure the range over which to collect data was wide enough to capture the data effectively, whilst constraining conditions to avoid ACC damage and discoloration at extreme conditions of time and temperature. Six center points (CPs) runs were included to provide sufficient degrees of freedom, comprising a combination of the mid-points of all factor settings. Table 1 outlines the continuous factors and their coded values. Runs were conducted for both F0 and F1 systems, therefore, the use of the interleaf film is included as a categorical factor. A representation of the full factorial design domain is shown in Fig. 2(a). For compaction temperature, a lower limit of 30 °C was chosen to allow accurate maintenance in the laboratory environment, and an upper limit of 120 °C was chosen to avoid damage of the ACCs which was found to occur beyond this point. To determine the range of times to be explored, several preliminary samples were made at 120 °C, and it was found that the Tencel based ACCs were not damaged if processed at a maximum of 180 min.

Table 2 shows the experimental runs used in this study. The first 14 runs comprise the original full factorial design which includes 8 factorial runs (corner points) and an additional 6 center point repeat samples (CPs). The center points are located at the mid-point of all factor ranges

Table 1
Factors used in the full factorial design. Actual values used in the experiment are shown, and coded values are displayed in brackets.

Continuous Factors	Lower (−1)	Centre Point (0)	Upper (1)
A: Temp (°C)	30	75	120
B: IL%	30	65	100
C: Time (mins)	10	95	180
Categorical Factor			
Film	No (F0)		Yes (F1)

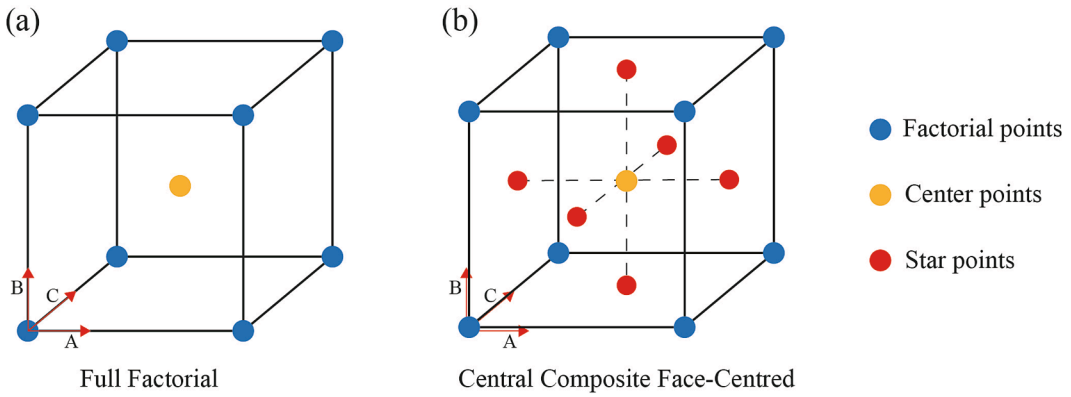

Fig. 2. Geometry of the full factorial (a) and central composite face centered (CCF) (b) design spaces with three factors (A,B,C) with associated experimental runs. The factorial/corner points and center points are shown as blue and yellow dots respectively. Additional runs (star points) for the CCF are shown as red dots.

Table 2
Experimental runs used in the study and listed in the run order. IDs for ACCs made with film, and without film are prefixed with 'F1′ and 'F0′ respectively. The first 14 lines represent the full factorial design and the last six lines (in bold) represent the additional CCF runs.

ID (Film)	ID (No Film)	Factor settings		
		A	B	C
F1_1(CP)	F0_1(CP)	75	65	95
F1_2	F0_2	30	30	10
F1_3(CP)	F0_3(CP)	75	65	95
F1_4	F0_4	120	30	180
F1_5	F0_5	30	30	180
F1_6	F0_6	120	100	10
F1_7(CP)	F0_7(CP)	75	65	95
F1_8	F0_8	30	100	180
F1_9	F0_9	120	30	10
F1_10	F0_10	120	100	180
F1_11(CP)	F0_11(CP)	75	65	95
F1_12	F0_12	30	100	10
F1_13(CP)	F0_13(CP)	75	65	95
F1_14(CP)	F0_14(CP)	75	65	95
F1_15	**F0_15**	**30**	**65**	**95**
F1_16	**F0_16**	**120**	**65**	**95**
F1_17	**F0_17**	**75**	**30**	**95**
F1_18	**F0_18**	**75**	**100**	**95**
F1_19	**F0_19**	**75**	**65**	**10**
F1_20	**F0_20**	**75**	**65**	**180**

A = Temperature (°C), B = IL %, C = Time (mins)
Center point IDs are suffixed by (CP).

and are replicated to allow an assessment of repeatability and error estimation [39,41]. The order of runs to be conducted was randomized to reduce the risk of systematic errors. The data collected as part of the full factorial design was fitted to a linear model as shown in Eq. (1) for M independent factors, incorporating main effects and interactions. The predicted average response variable ($\hat{y}_i$) is expressed as a linear combination of the factors. These linear and interaction terms of the independent factor variables are represented by x_i, and x_ix_j, and β_0, β_i, and β_{ij}, represent the coefficients determined when fitting the model for the intercept, linear and interaction terms respectively.

$$\hat{y}_i = \beta_0 + \sum_{j=1}^{M}\beta_j x_j + \sum_{i<j}\sum_{j=1}^{M}\beta_{ij}x_i x_j \quad (1)$$

2.5.2. Response surface design

For further optimisation, a face-centered central composite (CCF) response surface design was used. This is a type of central composite design that can be established by expanding on the original full factorial design[37,42,46]. A further six experimental runs, known as star points, are added to allow quadratic effects to be estimated. With a face-centered design, the star points are located on the face of the experimental design cube, as shown in Fig. 2 (b). Each factor has three levels as outlined in Table 1 but the additional combinations provide more data to analyse. Equation (2) shows the response surface model, with the quadratic term x_i^2 included, β_{ii} representing the coefficients determined when fitting the model for quadratic terms.

$$\hat{y}_i = \beta_0 + \sum_{j=1}^{M}\beta_j x_{ij} + \sum_{i<j}\sum_{j=1}^{M}\beta_{ij}x_i x_j + \sum_{i=1}^{M}\beta_{ii}x_i^2 \quad (2)$$

An extra six samples were required to expand the original full factorial design, making a total of 20 runs as shown in Table 2.

2.6. Statistical analysis

The initial full factorial design and subsequent CCF design were generated using the software package Minitab. Regression analysis and analysis of variance (ANOVA) of the experimental data was also carried out using Minitab. Analysis was conducted separately for both systems (F0, ACCs without film and F1, ACCs with film) to allow comparison of these two systems and factor analysis to focus on the continuous factors of temperature, IL %, and time. Backward elimination of insignificant terms (p-value $\geq$ 0.05 considered insignificant) was used to generate a model to link the response variable to process factors. The goodness of fit of the model to the experimental data was assessed from calculation of coefficient of determination, R^2 [47–49]. This was supported by calculation of adjusted coefficient of determination, $R^2_{(adj)}$, used to validate the strength of model with respect to the number of model terms. The predictive power of the resulting model was gauged through calculation of predicted coefficient of determination, $R^2_{(pred)}$ [36].

2.7. Optimization and validation

Optimum process conditions to produce the most desirable response value were identified using Derringers desirability function [50], and samples were produced in the lab using these conditions. These samples were tested and resulting properties compared to the prediction, to assess how well the obtained model could predict ACC properties.

3. Results and Discussion

3.1. Initial analysis of the full factorial data

Tensile strength, Young's modulus and strain-to-failure were collected for the ACC samples produced for the full factorial design and are shown in Table 3. Both systems F1(with film) and F0(no film) are shown, with the average of each run taken from five test specimens. An average value from six center points (CPs) was calculated.

Young's modulus, tensile strength and strain-to-failure are plotted for each sample and shown in Fig. 3, in order of ascending Young's modulus with respect to the ACCs made with the film. Optical microscopy images of all prepared samples are shown in Fig 4 and Fig 5 for the F0 and F1 systems, respectively. Minimal differences in tensile strength are seen when comparing systems F0 and F1, suggesting that the film has little benefit on this property. In our previous work [43], we found there to be a small reduction (~ 5–10 MPa) in tensile strength when using the film at the fixed processing conditions used. Here, we find that this property remains relatively unaffected with respect to using the film. There is more variation in values across Young's modulus and strain-to-failure, however. Young's modulus values are higher when the film is not used, with an average increase of 1–2 GPa for majority of samples. F0 and F1 systems are seen to follow similar trends, however, this is particularly strong for strain-to-failure as shown in Fig. 3(c). The data from both systems displays consistent patterns with the same high-to-low order observed in both, suggesting that the film does not affect how the process conditions influence this property.

The sample produced at the lowest factor settings (F0_2/F1_2) exhibits the highest strain-to-failure, indicative of under processing, or reduced dissolution of the yarns, which would allow them to untwist and stretch out under applied load, resulting in a high strain-to-failure. This sample also exhibits the lowest Young's modulus, making it the least desirable ACC of those produced, with or without the interleaf film. This does not definitively suggest that these lower settings are insufficient to produce ACCs, but the combination of all three factors at low settings is unlikely to be optimum, resulting in a thicker cross-section, and less consolidation throughout as shown in Fig 4(a) and Fig 5(a).

Interestingly, the most desirable combination of properties is seen from the CPs which possess the highest Young's modulus and lowest strain-to-failure. Additionally, Fig 4 and Fig 5 show that the most consolidated cross-sections are indeed seen at the CPs, consistent with the improved properties when compared to the corner points. This initial analysis suggests that the region around the CPs may be most optimum for ACCs, irrespective of whether the film is used or not. Indeed, the samples with strain-to-failure values in the region of 4 % show better consolidation than those exhibiting higher values, as seen in samples F0_6, F0_8 and F0_10 (Fig 4 (d, g, h)) and samples F1_6 and

Table 3
Measured responses from the experimental runs of the full factorial design. F1_CPs and F0_CPs represent the average values over 6 center points for F1 and F0 systems, respectively.

ID	Factor Settings			Responses											
	A	B	C	Young's modulus (GPa)			Strain-to-failure (%)			Tensile Strength (MPa)			Density (g/cc)		
F1_2	30	30	10	1.7	±	0.0	15.4	±	0.3	56.7	±	1.3	0.97	±	0.03
F1_4	120	30	180	2.5	±	0.2	10.0	±	0.4	51.4	±	4.9	1.03	±	0.02
F1_5	30	30	180	2.6	±	0.0	12.9	±	0.7	59.1	±	2.0	1.01	±	0.01
F1_6	120	100	10	3.9	±	0.3	3.0	±	0.2	63.1	±	2.7	1.29	±	0.02
F1_8	30	100	180	3.2	±	0.3	5.9	±	0.5	56.9	±	3.9	1.21	±	0.01
F1_9	120	30	10	3.6	±	0.1	7.4	±	0.6	56.7	±	1.9	1.21	±	0.01
F1_10	120	100	180	3.5	±	0.8	2.5	±	0.4	58.3	±	3.6	1.32	±	0.01
F1_12	30	100	10	3.5	±	0.1	7.3	±	0.8	50.7	±	2.1	1.16	±	0.02
F1_CPs	**75**	**65**	**95**	**4.6**	**±**	**0.4**	**2.2**	**±**	**1.1**	**59.6**	**±**	**3.3**	**1.27**	±	**0.02**
F0_2	30	30	10	1.8	±	0.2	10.8	±	1.0	46.5	±	2.1	0.98	±	0.02
F0_4	120	30	180	3.4	±	0.1	5.8	±	0.6	46.4	±	1.6	1.07	±	0.01
F0_5	30	30	180	4.7	±	0.2	7.4	±	0.1	60.9	±	1.7	1.19	±	0.03
F0_6	120	100	10	5.6	±	0.1	2.3	±	0.2	67.6	±	1.1	1.21	±	0.03
F0_8	30	100	180	5.1	±	0.3	3.0	±	0.0	59.1	±	1.4	1.23	±	0.02
F0_9	120	30	10	3.0	±	0.2	6.3	±	0.1	44.7	±	1.4	1.03	±	0.03
F0_10	120	100	180	5.3	±	0.2	2.1	±	0.1	64.8	±	1.6	1.25	±	0.01
F0_12	30	100	10	3.9	±	0.1	5.1	±	0.0	53.7	±	2.2	1.13	±	0.02
F0_CPs	**75**	**65**	**95**	**5.5**	**±**	**0.2**	**1.6**	**±**	**0.2**	**58.4**	**±**	**2.5**	**1.22**	**±**	**0.03**

A = Temperature (°C), B = IL %, C = Time (mins)

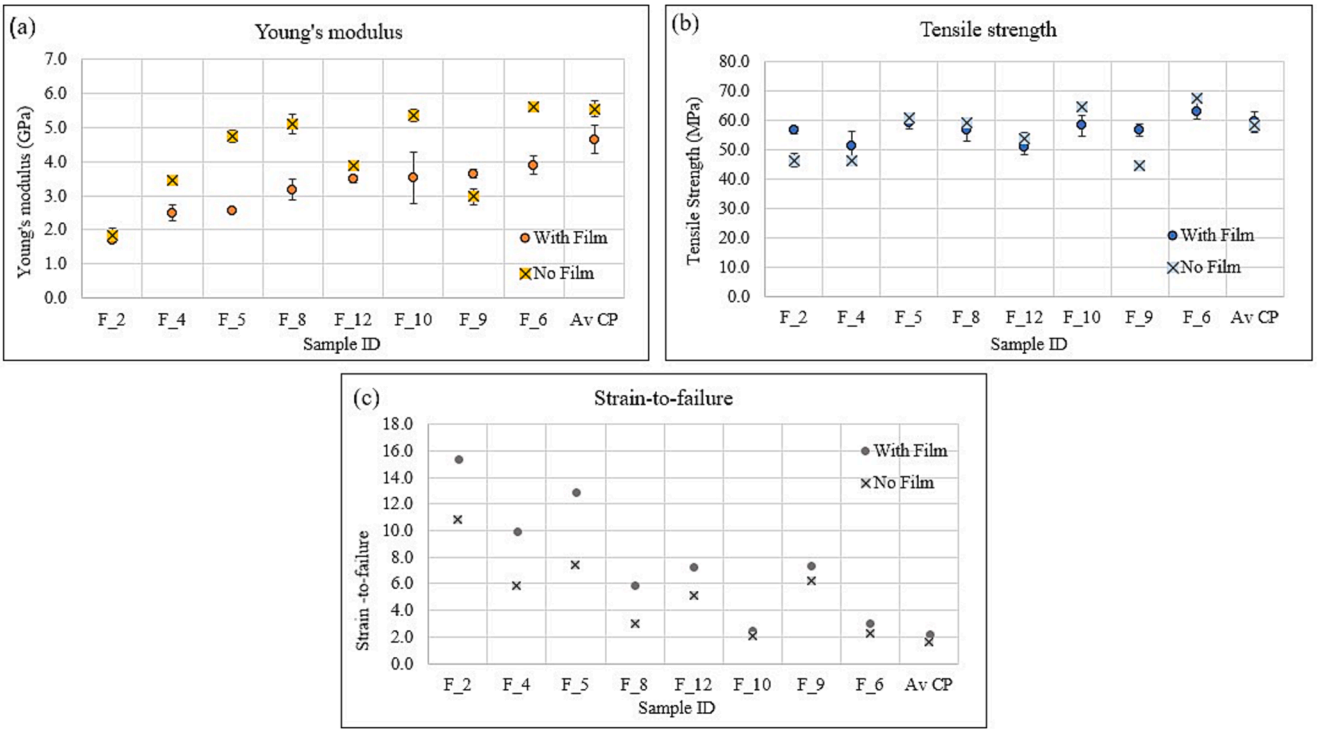

Fig. 3. Measured values for Young's modulus, YM (a), ultimate tensile strength, UTS (b) and strain to failure, STF (c) across all full factorial runs for ACCs made with film (solid dot) and no film (cross-box).

F1_10 (Fig 5 (g,h)), coinciding with the increased Young's modulus values. We suggest that higher strain-to-failure values are attributed to poor bonding within the composite structure. An unprocessed fibre in the ACC could, therefore, stretch more under applied strain, giving a higher strain-to-failure of the overall ACC. Additionally, whilst the strain-to-failure of Lyocell fibres is in the region of 20 % [51,52], a matrix produced from Lyocell fibres is in the region of 4 % [52], which supports the observations. This suggests that a strain-to-failure in the region of 4 % can be used as a guide, to achieve good consolidation between the fibre and matrix phases indicative of sufficient processing in the ACCs.

3.2. Presence of the film

Another crucial observation emerging from Fig 5 is that the film layer can still be clearly seen. This was not the case in our previous work in cotton-based ACCs [33] where it was found that when the film fully dissolved, the matrix component provided by the film could penetrate the fibre assembly as well as sit between the textile layers. This reinforced intralayer and interlayer bonding within the material, which contributed to improved mechanical properties when compared to a scenario where the film only partially dissolved. It is possible that the process conditions obtained through the full factorial design are not sufficient to achieve full dissolution of the film. Many samples are under

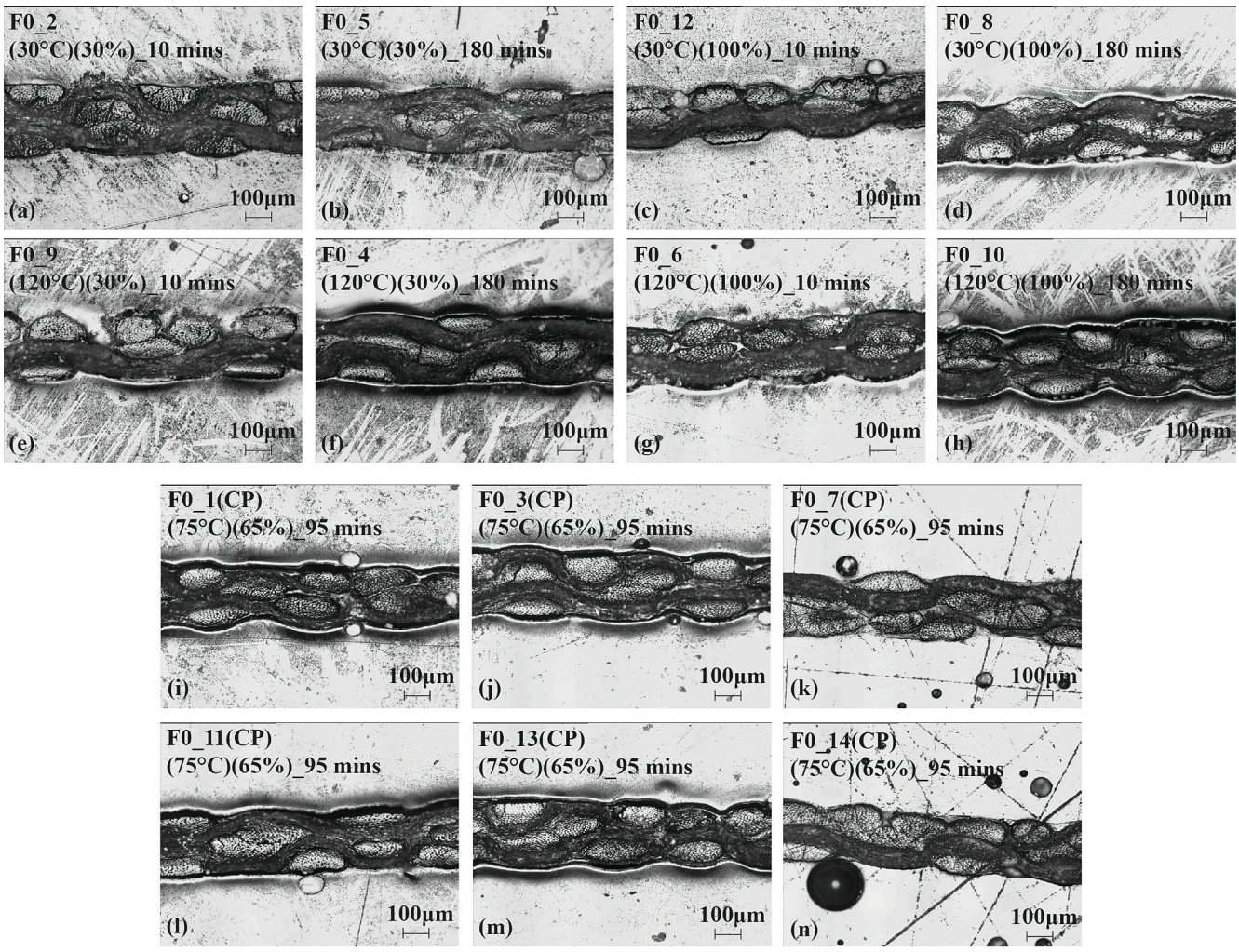

Fig. 4. Optical micrographs of the full factorial corner points (a-h) and center points (i-n) for the F0 system.

processed with large strain-to-failure values, where it may be expected that the film would not fully dissolve, however, the film is visible across all FF samples including the six CPs which possess the best balance of properties. It is, therefore, entirely possible that there is an optimal region not captured yet from the full factorial design, something to bear in mind as we conduct the ANOVA analysis.

3.3. ANOVA analysis of the full factorial data

ANOVA analysis was conducted using the data obtained through the full factorial design for both F0 and F1 systems separately and is provided in the supplementary information (Tables S1-S3). To summarize, it was possible to capture strain-to-failure in some capacity for both systems, however, the fit of the model to the data was not strong as indicated by low coefficient of determination (R^2) values of 37 % and 50 % for the F0 and F1 systems respectively. Young's modulus was captured only for the F0 system, however, again, the model was not a good fit to the data, as evidenced through a low R^2 value of 30 %.

Center points are valuable additions to experimental designs such as the full factorial design as they can provide indication of the reproducibility of a process and an estimation of error [39,41]. In addition, the presence of CPs can also offer insight into possible quadratic effects of factors that the full factorial alone cannot capture. Whilst inconclusive, the results of the ANOVA are unsurprising given the best balance of Young's modulus and strain-to-failure is observed at the CPs. A full factorial study can capture only linear relationships with interactions, as there is not enough data to estimate quadratic effects. It can, however, give some indication that there may be curvature, as indicated by a significant p-value ($p < 0.05$) associated with possible curvature. This was observed for strain-to-failure across both systems, consistent with the lack of fit of the captured linear model and is also the case for Young's modulus for the F0 system. It is, therefore, recommended to expand to a CCF design to explore the design space further across both F0 and F1 systems.

3.4. Initial analysis central composite face centered design (CCF)

As illustrated in Fig. 2 (b), the experimental runs of the CCF comprise those of the original full factorial design, plus an additional 6 runs. The results are presented in Table 4. Density and strain to failure are plotted against Young's modulus for the ACCs prepared without film (system F0) and presented in Fig. 6. Here, all the results from the full factorial, CCF and CPs fall on the same straight line. The CPs fall in a more desirable region (higher Young's modulus, lower strain-to-failure, higher density) than the corner points of the FF, and the six centre face points from the CCF (red points) are overall better than the CPs, revealing a new optimal region where the Young's modulus is the highest. This region was not revealed previously in the original full factorial design runs (blue), nor was it occupied by the centre points (orange). Whilst arguably unsurprising, the advantage of expanding a full factorial design to a response surface design is highlighted here, where additional samples can start to narrow down the region of

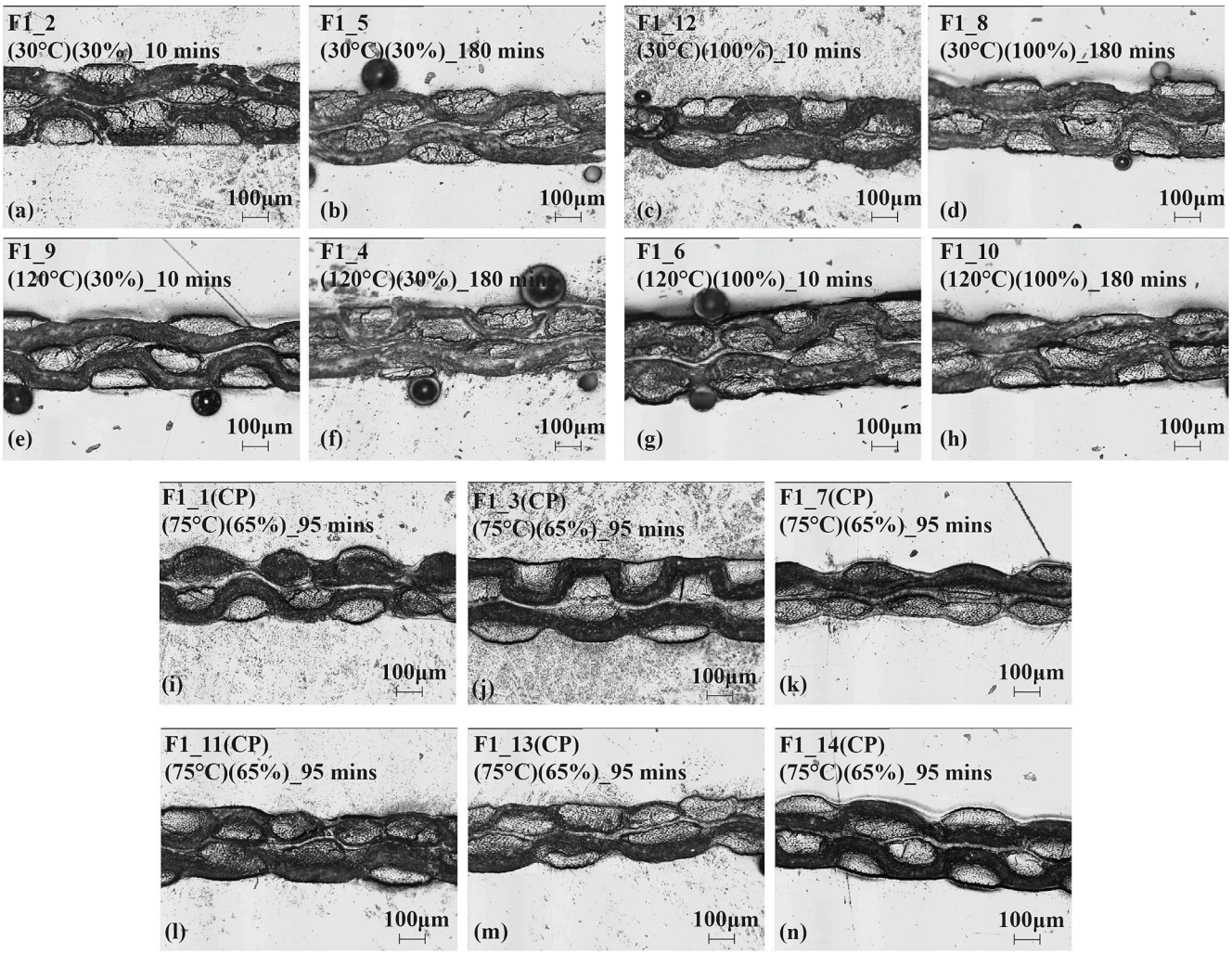

Fig. 5. Optical micrographs of the full factorial corner points (a-h) and center points(i-n) for the F1 system.

Table 4
Measured responses from the six additional experimental runs produced to form the CCF.

ID	Factor Settings			Responses											
	A	B	C	Young's modulus (GPa)			Strain-to-failure (%)			Tensile Strength (MPa)			Density (g/cc)		
F1_15	30	65	95	6.0	±	0.2	2.1	±	0.3	57.8	±	1.6	1.31	±	0.01
F1_16	120	65	95	6.0	±	0.3	1.4	±	0.1	63.3	±	0.9	1.25	±	0.00
F1_17	75	30	95	3.4	±	0.1	8.8	±	0.8	56.4	±	3.1	1.10	±	0.02
F1_18	75	100	95	5.6	±	0.1	1.7	±	0.2	60.1	±	2.5	1.33	±	0.01
F1_19	75	65	10	5.5	±	0.1	1.5	±	0.1	59.5	±	3.2	1.25	±	0.02
F1_20	75	65	180	6.7	±	0.03	1.2	±	0.02	62.4	±	1.1	1.32	±	0.02
F0_15	30	65	95	5.5	±	0.3	1.8	±	0.1	53.5	±	2.6	1.18	±	0.02
F0_16	120	65	95	6.1	±	0.2	1.6	±	0.02	64.8	±	3.5	1.18	±	0.02
F0_17	75	30	95	6.2	±	0.1	3.0	±	0.2	59.4	±	0.6	1.27	±	0.02
F0_18	75	100	95	5.9	±	0.2	1.7	±	0.2	62.9	±	3.0	1.25	±	0.02
F0_19	75	65	10	5.5	±	0.4	1.5	±	0.01	57.6	±	2.8	1.26	±	0.00
F0_20	75	65	180	6.3	±	0.1	1.4	±	0.2	68.0	±	4.8	1.27	±	0.01

A = Temperature (°C),
B = IL %, C = Time (mins)

optimisation from the initial experimental domain. Prior to statistical analysis of the data, it could be suggested that the optimized region bears similarities to the processing conditions of the CPs, i.e., the mid-points. Perhaps a combination of mid-point factor settings leads us to more desirable ACCs, suggested by the CFF, which offers more precision.

Optical micrographs of the six experimental runs for the F0 system are presented in Fig. 7. The additional samples exhibit improved consolidation when compared to the eight corner points of the full factorial (Fig 4). Similar observations are seen with the F1 system as shown in Fig. 8, however, the CCF runs are not in line with the trend observed from the FF data. Instead, they have their own correlation, evidencing the curvature in the data that was not picked up from the full factorial points alone. Indeed, the CCF expansion has captured a region of processing conditions where, for the F1 system, Young's modulus is

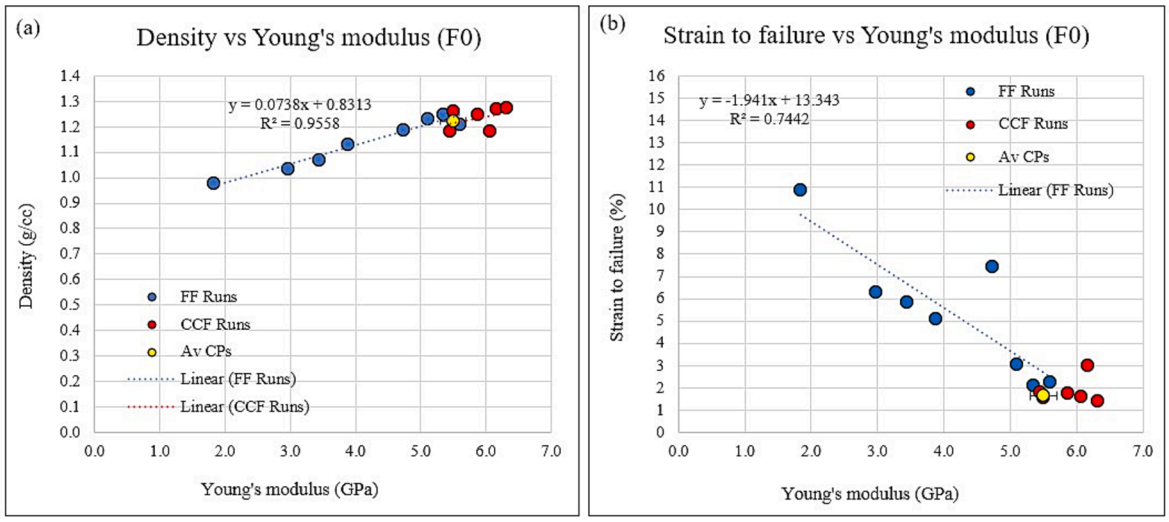

Fig. 6. Density (a) and strain to failure (b) are plotted against Young's modulus for all runs in the CCF design for ACCs made without film (F0). Corner points from the full factorial design are shown in blue, The average CP value is shown in orange, and the additional CCF runs are shown in red.

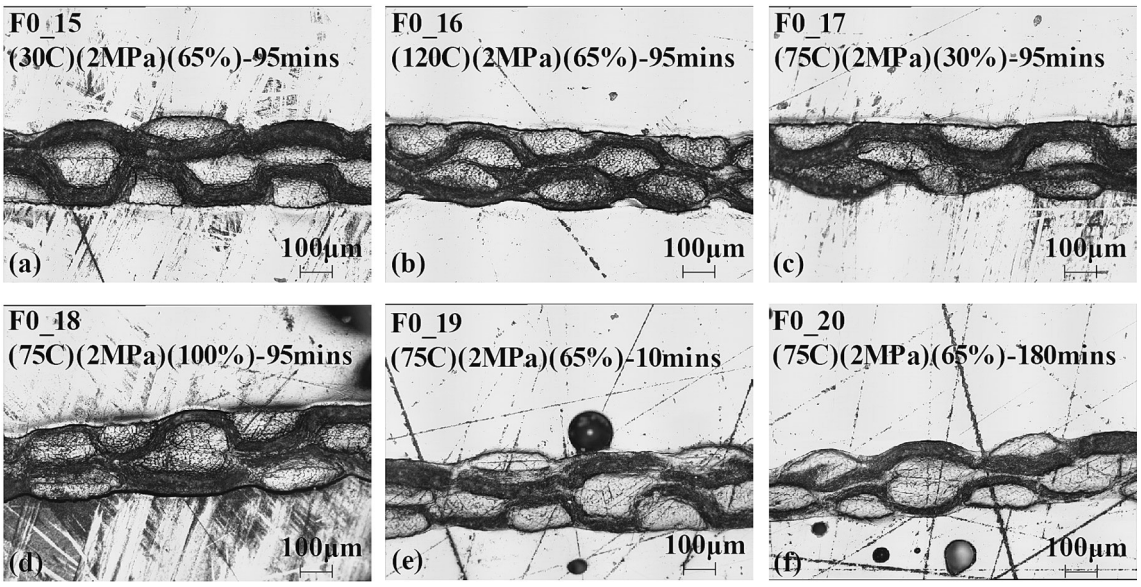

Fig. 7. Optical micrographs of six additional samples (F0 system) prepared for the CCF.

more sensitive to changes in density. This is highlighted through the decreased gradient of the trendline captured for the CCF data. For both systems, the highest Young's modulus is achieved with sample F0_20 and F1_20, with values of 6.3 GPa and 6.7 GPa respectively. Here, both temperature and IL % are at the mid-points, however, the increased time to 180 min helps to increase Young's modulus beyond that achieved at the CPs. It could be that more time is needed to push the internal air out from the sample as we observed in our previous published work on cotton. F0_20 is visibly flatter from looking at Fig. 7, however from Fig. 10, F1_20 is comparable in in thickness to the rest of the samples. The additional CCF samples made with film (F1) are presented in Fig. 9 and the same observation is made is from the extra CCF samples as previously, where the film can be seen in between the layers. We postulated that the film may only be partially dissolving at the process conditions assigned by the FF design, and by exploring the design space further, we could close in on a more optimum region where the film fully dissolves, forming a more consolidated ACC with better properties. The extra samples do exhibit better properties; however, the film is still visible, leading us to rethink the film behavior in the context of the textile, or more specifically, the Tencel fibre structure. It is possible that the layer seen is in fact, dissolved cellulose that has remained in between the textile layers, and on coagulation, has formed a layer of matrix component, and this is supported by our previous works [33,43] reporting on ACCs prepared using cotton textiles. From this work we can identify a handful of samples prepared with cotton textile, at comparable processing conditions to those used in this work.

Fig. 10 shows optical microscopy images of ACCs prepared using cotton textile and interleaved films at 100 °C, 2 MPa for 10 min, using 60 and 70 % IL in DMSO. Here we note that full dissolution of the film has occurred. This is not the case for sample F1_16 shown in Fig. 9(b), which was prepared at similar IL concentrations. This sample was prepared at 120 °C for 95 min, which would support more, rather than less, dissolution of the film. This suggests that the film has indeed dissolved fully, but the fact that we can still see a distinct region between the textile layers suggests that whilst the film dissolved, it had nowhere to go, and coagulated to form matrix exactly where it was placed during preparation. In our previous work [33], the film was found to significantly improve interlaminar bonding, but in order to do so, it had to at least

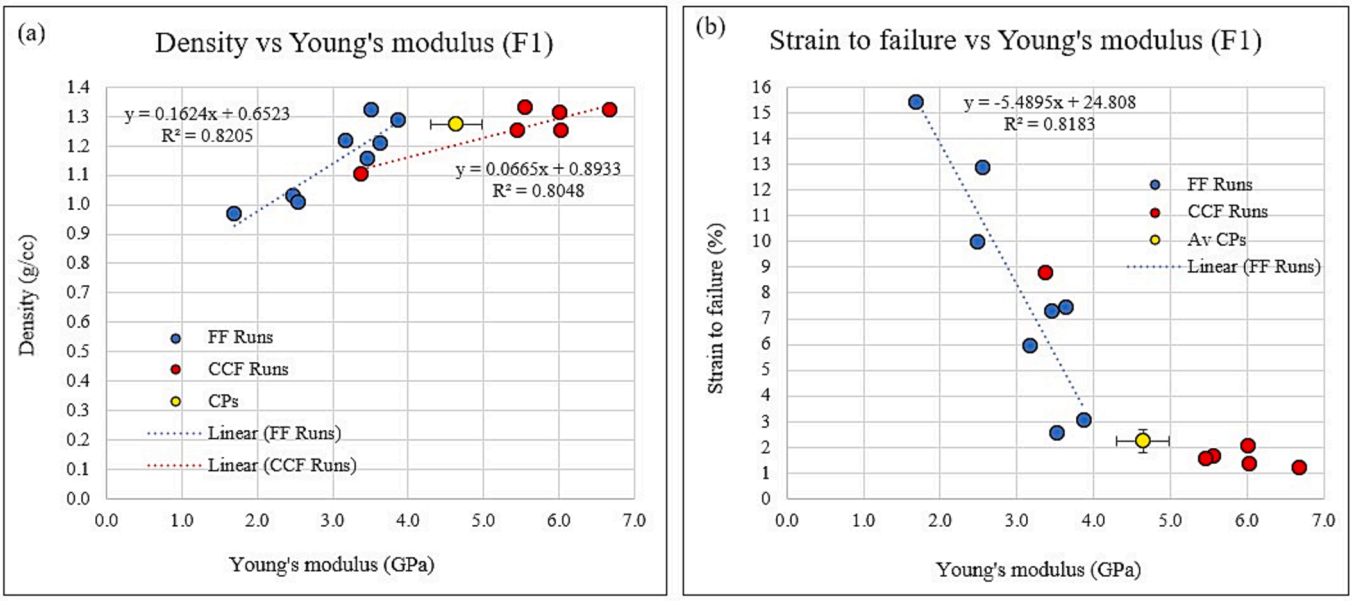

Fig. 8. Density (a) and strain to failure (b) are plotted against Young's modulus for all runs in the CCF design for ACCs made with film (F1). Corner points from the full factorial design are shown in blue. The average CP value is shown in yellow, and the additional CCF runs are shown in red.

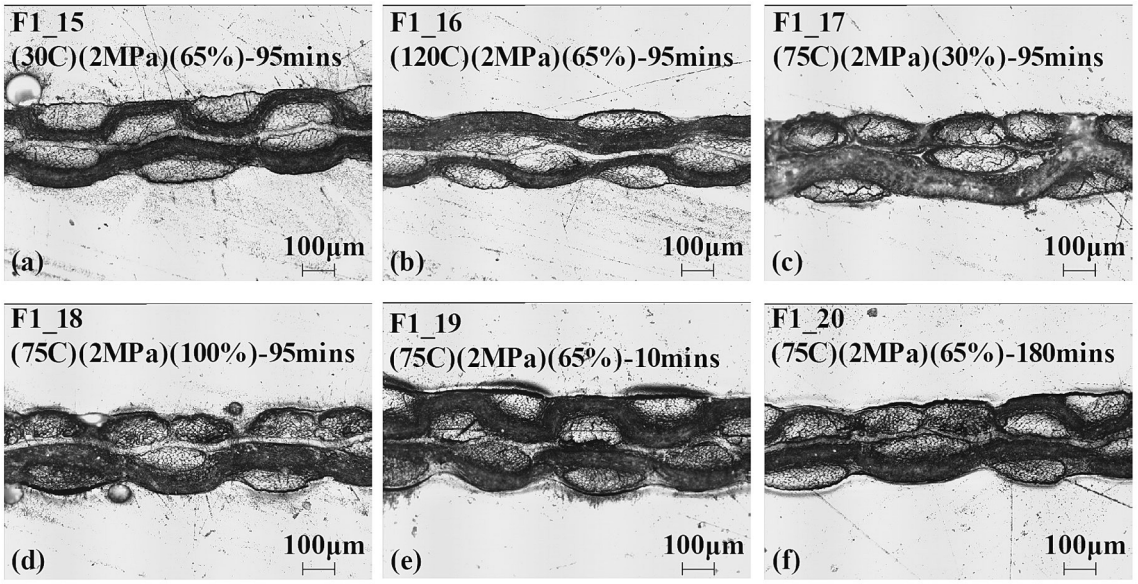

Fig. 9. Optical micrographs of six additional samples (F1 system) prepared for the CCF.

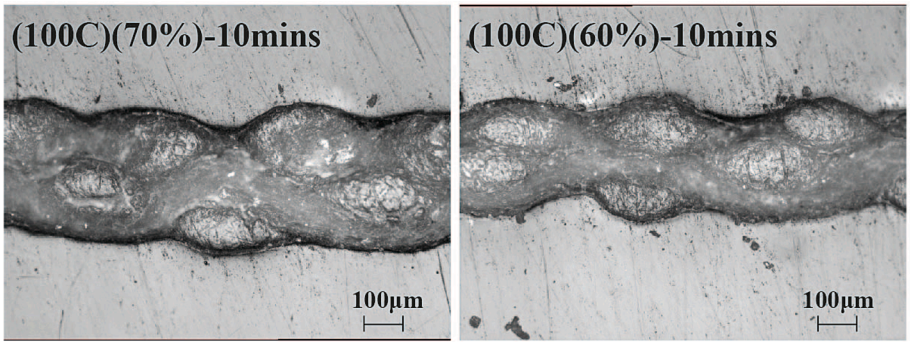

Fig. 10. Optical microscopy images of ACCs from previous work [33] prepared using cotton textile and interleaved films.

partially dissolve in order to support a strong interface and avoid delamination. It didn't necessarily need to penetrate through the textile to improve bonding, however, its mere presence provided the composite with enough matrix to bond the layers together which resulted in a significant increase in peel strength. What we did find, was that a 3:1 S/C ratio (as used in this work) resulted in an ACC with the optimum Young's modulus as well as interlaminar bonding. This was associated with the film penetrating through the fibre assembly, supporting consolidation within the material, contributing to fibre–matrix bonding, and thus enhanced mechanical properties. Of the 20 samples prepared for the F0 and F1 systems, 18 comparative samples exhibited the same failure upon tensile testing, suggesting that overall, inter layer and intra layer bonding wasn't significantly influenced by the use of the film. Four samples delaminated upon testing for both F0 and F1 systems, and these samples were all processed at 30 % IL, the minimum setting for this parameter. The presence of the dissolved film provides insight into the Tencel fibers, as compared to the cotton fibers used in previous work. Tencel fibers are made up of multiple filaments, bundled together to form a fiber that is then woven into textile form. The filament cross section is largely spherical and smooth [53–55], allowing them to pack together more closely that in a native yarn such as cotton, which is made up of many bundles of irregular shaped cotton fibers [54,56]. This offers more space between the fiber bundles for solvent to access during dissolution, whereas in Tencel, the packing makes it harder for solvent to access. The reduced accessibility of the filament bundles possibly explains why the film is still seen in the ACCs, rather than dissolving and penetrating through the fibers as we saw in cotton-based ACCs. In the case of the Tencel, the film dissolves but is unable to move as easily. On coagulation, it remains in between the textile layers.

3.5. ANOVA analysis central composite face centered design (CCF)

The CCF data for each system (F0, F1) was analysed separately using Minitab. The extra CCF runs did not help to capture tensile strength, however, this is unsurprising given the small range of values across all 20 runs. This was the case for both systems, suggesting that this property is not sensitive to the processing conditions or the addition of the film. The F0 system was not captured well for strain-to-failure or Young's modulus as evidenced by poor fit statistics. The results are presented in the supplementary information (Tables S4-S5) but to summarize, a quadratic relationship was fitted to strain-to-failure, but the model had a significant lack of fit (F-value < 0.05). Young's modulus was also captured in a quadratic model; however, this was associated with a low predicted coefficient of variance ($R^2_{(pred)}$) of 21 %. The poor fit statistics put into question the predictive ability of the models captured. The additional runs, however, did allow the data from the F1 system to be captured across both Young's modulus and strain-to-failure.

3.5.1. Young's modulus (F1 system)

Young's modulus was fit to second order quadratic model as shown in Equation (3). The equation is shown in the form of uncoded factors where B represents IL %, the only significant factor identified for this property. This suggests that the film may reduce the sensitivity of mechanical properties to the processing parameters.

$$Young's\ modulus(GPa)(F1) = -2.33 + 0.2152B - 0.001526B^2 \quad (3)$$

The results of the ANOVA analysis for the F1 system are presented in the supplementary information (Table S6). If the p-value associated with each factor and factor combination is less than 0.05, this indicates a significant effect within a confidence range of 95 % [48], which can be seen in the ANOVA tables. The model has a good fit to the experimental data as indicated by the p-value ($p < 0.05$) for the model indicator [37,48,49]. Furthermore, there is no significant lack of fit, as highlighted by the associated p-value ($p < 0.05$), and F-value (> 1) which indicates confidence in the models [36,49]. The model derived through the F1 system agrees well with the data obtained as indicated by the $R^2_{(adj)}$, and $R^2_{(pred)}$ values, where the difference between these values is less than 0.2 [48,49,57–59]. This was not the case for the F0 system. A main effects plot is provided in the supplementary information (Fig S1), displaying the proposed effect of IL% on Young's modulus. This suggests that the optimum IL% for maximizing this property is 70 %. This is similar to the concentration used in our previous work of 80 %, which we determined through an OFAT approach [33]. A sufficient amount of ionic liquid is required to process the ACCs and achieve good bonding between the fibres and the matrix. However, the addition of DMSO is beneficial to allow ease of application of solvent solution to the ACC stack through lowering its viscosity.

3.6. Strain-to-failure (F1 system)

It was possible to capture strain-to-failure and the results of the ANOVA analysis for this property are shown in the supplementary information (Table S7). Equation (4) represents the second order quadratic models for the F1 system. As before, the equation is shown in the form of uncoded factors where A and B represent temperature in °C, and IL %, respectively. Here, we see that strain-to-failure has a temperature dependance, but again as with Young's modulus, time has not been identified as significant. The difference between the $R^2_{(adj)}$, and $R^2_{(pred)}$ values is less than 0.2 and the model indicator shows a good fit to the experimental data ($p < 0.05$).

$$Strain - to - failure(\%)(F1) = 30.54 - 0.0427A - 0.6834B + 0.004509B^2 \quad (4)$$

In summary, the CCF data has helped further identify the significant terms across the properties of Young's modulus and strain-to-failure for the F1 system, where no terms were found in the original FF design. Through the CCF we now obtain information to suggest that IL% plays a role in driving this property. Additionally, the terms of temperature and IL% originally identified in the FF are still identified through the CCF, and the additional quadratic effect of IL% has improved the strength of the derived model from before. Interestingly, time has not been identified as significant in driving ACC properties, in contrast to our previous work on cotton-based ACCs [43]. It was found that whilst dissolution of the film layer was not time-dependent, Young's modulus did improve with increased time, up to a point. Over time, internal air will be pushed out, increasing the density of the resultant ACC. If time was increased further, a decrease in properties resulted, and we hypothesized that this was due to increased fibre dissolution combined with excess matrix being pushed out. With a Tencel-based ACC, film dissolution is achieved in all ACC samples, and time is not identified as being influential. The data for the two properties was captured more strongly for the F1 system, supporting an optimisation stage, so it was decided that a multi-response optimisation would be performed across this system on the derived models for Young's modulus and strain-to-failure, using Derringer's Desirability function.

3.7. Optimisation

Derringer's desirability function was used to obtain a combination of significant process factors to yield the best balance of Young's modulus and strain-to-failure for ACCs made with film. The aim here was to maximise Young's modulus and maintain strain-to-failure around 4 % to avoid under processing as seen in earlier samples. The processing conditions with the predicted values for Young's modulus and strain-to-failure are outlined in Table 5. It is interesting to note that time was deemed insignificant in driving both Young's modulus and strain-to-failure for the F1 system, which was suggested earlier on analysis of the FF data. The majority of the extra six samples have indeed higher Young's modulus values and strain-to-failures below 4 % and were produced at three different time settings. With this in mind the data

Table 5
Optimum processing conditions obtained through the response surface models for Young's modulus and strain-to-failure, for ACCs prepared with interleaf film.

Processing conditions	With Film system
A: Temperature (°C)	30
B: IL (%)	70
C: Time (mins)	10*
Predicted responses	
Young's modulus (GPa)	5.3
Strain-to-failure (%)	3.5 %
Desirability	0.76
* denotes arbitrary setting for insignificant factors	

arguably lends itself to this possible conclusion, however, there is a difference of 1.2 GPa between samples F1_19 and F1_20, processed at the same temperature and IL%, but for 10 and 180 min respectively. Furthermore, the predicted response for Young's modulus is 5.25 GPa, which is lower than 5 of the extra 6 samples produced for the CCF. Multi-response optimisation can result in a compromise between responses to get the best overall desirability, however, in this case Young's modulus is driven by only IL%. Both responses rely on IL % to drive them, and optimize at 70 %, however, the inclusion of temperature originates from the model for strain-to-failure only. Therefore, the model irrespective of strain-to-failure would predict an optimum Young's modulus of 5.25 GPa. Nevertheless, the data has led to the predicted responses, and it is worthwhile to see if this can be validated. As time was deemed insignificant for the F1 system, a time of 10 min was chosen for validation. Four replicates were made, with four specimens tested from each replicate. The mean, and coefficient of variance across all replicates was then calculated.

3.7.1. In-lab model validation

The measured properties of the four in-lab test samples are shown in Table 6, along with coefficient of variance (COV) and standard deviation cross the four replicates prepared with film. An independent two-sample *t*-test ($p = 0.05$) was conducted to compare the means of the model prediction, and the experimental samples. The test concluded that the difference between the means for both Young's modulus and strain-to-failure was not significant, thus validating the relationships found between process conditions and both mechanical property responses. The use of interleaf films appears to lead to a process that can be modelled with predictive capability for mechanical properties such as Young's modulus and strain-to-failure. A comparison of mechanical and physical properties of the optimised ACCs produced in this work, and optimised ACCs produced in our previous work, is provided in the supplementary information (Table S8).

3.8. Discussion

The adequacy of the model derived from the CCF has been confirmed through comparison to in-lab samples, however, it is important to acknowledge the possibility that there may be a better region in the experimental space to optimize mechanical properties, that the CCF has not identified. This is due to the notably higher measured values of the experimental runs used to expand the FF design to the CCF. The CCF approach is efficient for reducing experimental runs as it builds on an FF design, and it also allows the mid-points of factors to be explored in combination with more extreme values. Central composites designs typically have this attribute, for example a central composite circumscribed (CCC) design, however, this often involves expanding the design space itself, which would result in negative factor settings in our case. The CCF option allows star points to sit within the space, as well as make use of an existing FF design. Given that some corner points of the FF exhibited similar favorable properties to the CPs, it was a reasonable strategy to consider the CCF approach to explore whether an optimized region lay directly near the CPs, or in some combination of factor mid-points. It is also important to acknowledge the limitations in the experimental work at lab scale and whilst every effort is taken to ensure samples are produced consistently (as demonstrated through replicates of CPs and validation samples), there may be specific disturbances (noise factors) that have yielded lower than expected experimental results, which would limit optimization. It is possible that noise may be too large due to the inherent capabilities of the experimental set up, meaning that predictions cannot be made within a small uncertainty window. The statistics have allowed us, nevertheless, to traverse the design space.

The noteworthy finding here is the ability of the F1 system to be modelled, where the F0 system was less successful. It is suggested that the film may help to maintain consistent dissolution conditions during sample making and, therefore, manage uncontrolled variability that arises through flashing. In essence, the film plays a role in reducing noise, thus allowing the ACCs to respond solely to the process factors under investigation. We observe the film remaining in between the textile layers which leads us to hypothesize that the structure of Tencel offers little space for it to migrate. This means that any dissolved cellulose from the fibres or film is likely to remain at the filament surface or in between the layers, rather than impregnating the filament bundles. Indeed, it may be that the fibre dissolution occurs only at the filament surface where it can be accessed easily. This means that the dissolved cellulose available for matrix is located such that it can leave the stack easily through flash, more so than if it were impregnating the filament bundles. In our previous work on cotton-based ACCs we showed that using enough solvent could offset flashing and provide enough matrix for consolidation [33]. With the Tencel textile, it may be that by off-setting the flash supports consistent matrix formation.

4. Conclusion

A design of experiments (DoE) approach was taken to investigate the processing of ACCs using Tencel textile and interleaved films, through the expansion of a full factorial screening to a central composite face centered (CCF) response surface design. It was found that the addition of the interleaved film allowed the process to be captured across the mechanical properties of Young's modulus and strain-to-failure, and a relationship between process conditions and mechanical properties was found. Validation samples were made at a temperature of 30 °C with 70 % IL as identified through multi-response optimisation which exhibited an average Young's modulus of 4.9 ± 0.2 GPa, and strain-to-failure of 3.3 ± 0.3 %. With model predictions of 5.3 GPa and 3.5 % respectively, the predictive ability of the relationship was confirmed, however, several samples in the CCF design were seen to exhibit higher Young's modulus values, leading us to question whether the 'true' optimum is yet to be found. An important discovery from this work is the behavior of the film and its role when applied to Tencel, and how this differed from

Table 6
Young's modulus and strain-to-failure of F1 experimental samples prepared at the identified optimum conditions, with model predictions.

Young's modulus (GPa)					Strain-to-failure (%)				
Prediction		Measured			Prediction		Measured		
Average	S.D	Average	S.D	COV	Average	S.D	Average	S.D	COV
5.3	0.9	4.9	0.3	5.3 %	3.5	1.5	3.3	0.5	13.6 %

previous work into native cotton-based ACCs [43], offering insight into how the structure of Tencel influences the resulting ACC. Here, the interleaf film dissolves during the process and forms a coagulated matrix region in between the textile layers, rather than penetrating the fibre assembly as observed with native cotton textile [33]. Whilst this additional matrix was not seen to improve or reduce ACC mechanical properties, the film provides an immediate supply of dissolved cellulose to the ACC that helps to offset flashing and contribute to more consistent ACC formation, that can be modelled across multiple factors. The use of DoE to accelerate ACC process understanding is crucial for future commercialization, and the insights gained from this work are important for the cellulose community and indeed, those working in natural fibre composites. This work additionally demonstrates the potential of regenerated cellulose fibers in the production and optimization of ACCs and highlights an application area for sustainable materials produced from end-of-life textiles. Future work will involve further exploration of alternative designs to more finely pinpoint the optimal space and identify how best to achieve the most desirable ACCs using Tencel, with expansion of the factor space to include other regenerated fibres such as viscose and indeed those produced from waste textiles.

CRediT authorship contribution statement

Ashley Victoria: Writing – review & editing, Writing – original draft, Validation, Methodology, Investigation, Formal analysis, Data curation, Conceptualization. **Peter John Hine:** Writing – review & editing, Supervision, Project administration, Methodology, Conceptualization. **Keeran Ward:** Writing – review & editing, Validation, Supervision, Project administration, Methodology, Conceptualization. **Michael Edward Ries:** Writing – review & editing, Validation, Supervision, Resources, Project administration, Methodology, Funding acquisition, Conceptualization.

Declaration of competing interest

The authors declare that they have no known competing financial interests or personal relationships that could have appeared to influence the work reported in this paper.

Data availability

Data will be made available on request.

Acknowledgements

The authors would like to thank Dr. Daniel L. Baker, Experimental Officer in the school of Physics and Astronomy, University of Leeds for experiment training and instruction. This research was supported through a studentship supported by the Engineering and Physical Sciences Research Council (EPSRC) Centre for Doctoral Training in Molecules to Product (EP/SO22473/1). The authors greatly acknowledge their support of this work.

Appendix A. Supplementary data

Supplementary data to this article can be found online at https://doi.org/10.1016/j.compositesa.2024.108510.

References

[1] Baghaei B, Compiet S, Skrifvars M. Mechanical properties of all-cellulose composites from end-of-life textiles. J Polym Res 2020;27(9).
[2] Chen F, et al. Unidirectional All-Cellulose Composites from Flax via Controlled Impregnation with Ionic Liquid. Polymers (Basel) 2020;12(5).
[3] Halley P. Sustainable Plastics Inspired by Nature. Physics 2020:13.
[4] Huber T, et al. Solvent infusion processing of all-cellulose composite materials. Carbohydr Polym 2012;90(1):730–3.
[5] Huber T, Pang S, Staiger MP. All-cellulose composite laminates. Compos A Appl Sci Manuf 2012;43(10):1738–45.
[6] Rosenboom JG, Langer R, Traverso G. Bioplastics for a circular economy. Nat Rev Mater 2022:1–21.
[7] Spörl JM, et al. Ionic Liquid Approach Toward Manufacture and Full Recycling of All-Cellulose Composites. Macromol Mater Eng 2018;303(1):1700335.
[8] Uusi-Tarkka E-K, Skrifvars M, Haapala A. Fabricating Sustainable All-Cellulose Composites. Appl Sci 2021;11:21.
[9] Wang J, et al. Towards a cellulose-based society: opportunities and challenges. Cellul 2021.
[10] Baghaei B, Skrifvars M. All-Cellulose Composites: A Review of Recent Studies on Structure, Properties and Applications. Molecules 2020;25(12).
[11] Gindl W, Keckes J. All-cellulose nanocomposite. Polymer 2005;46(23):10221–5.
[12] Nishino T, Arimoto N. All-Cellulose Composite Prepared by Selective Dissolving of Fiber Surface. Biomacromolecules 2007;8:2712–6.
[13] Zhao Q, et al. Novel all-cellulose ecocomposites prepared in ionic liquids. Cellul 2008;16(2):217–26.
[14] Nishino T, Matsuda I, Hirao K. All-Cellulose Composite. Macromolecules 2004;37:7683–7.
[15] Tanpichai S, et al. Review of the recent developments in all-cellulose nanocomposites: Properties and applications. Carbohydr Polym 2022;286:119192.
[16] Mat Salleh M, et al. Parametric optimization of the processing of all-cellulose composite laminae. Adv Manuf Polym Compos Sci 2017;3(2):73–9.
[17] Alanazi M, Ries ME, Hine PJ. Dissolution of viscose rayon multifilament yarn in the ionic liquid 1-ethyl-3-methylimidazolium acetate studied using time–temperature superposition. Cellul 2023;30(14):8739–51.
[18] Preferred Fiber & Materials Market Report 2022. 2022..
[19] Moriam K, et al. Spinneret geometry modulates the mechanical properties of man-made cellulose fibers. Cellul 2021;28(17):11165–81.
[20] Rosenaua T, Potthasta A, Sixta H. The chemistry of side reactions and byproduct formation in the system NMMO/cellulose (Lyocell process). Prog Polym Sci 2001;26(1763–183).
[21] Preferred Fiber & Materials Market Report 2019. 2019..
[22] Wrap. Textiles market situation report 2019 2020;WRAP.
[23] Azimi B, et al. Cellulose-based fiber spinning processes using ionic liquids. Cellul 2022;29(6):3079–129.
[24] Harmsen, P. and H. Bos, *Textiles for Circular Fashion Part 1*. 2020.
[25] Haule LV, Carr CM, Rigout M. Preparation and physical properties of regenerated cellulose fibres from cotton waste garments. J Clean Prod 2016;112:4445–51.
[26] Asaadi S, et al. Renewable High-Performance Fibers from the Chemical Recycling of Cotton Waste Utilizing an Ionic Liquid. ChemSusChem 2016;9(22):3250–8.
[27] Ahmad SS, et al. The Application of Recycled Textile and Innovative Spatial Design Strategies for a Recycling Centre Exhibition Space. Procedia Soc Behav Sci 2016;234:525–35.
[28] Lee KE. Environmental Sustainability in the Textile Industry. In: Muthu SS, editor. Sustainability in the Textile Industry. Singapore: Springer Singapore; 2017. p. 17–55.
[29] Yadav R, Kamble Z. Textile waste-based cellulose composites: a review. J Mater Sci 2024.
[30] Baghaei B, et al. *All-Cellulose Composites Properties from Pre- and Post-Consumer Denim Wastes: Comparative Study*. Journal of Composites. Science 2022;6(5).
[31] Haslinger S, et al. Upcycling of cotton polyester blended textile waste to new man-made cellulose fibers. Waste Manag 2019;97:88–96.
[32] El Seoud OA, et al. Cellulose Regeneration and Chemical Recycling: Closing the "Cellulose Gap" Using Environmentally Benign Solvents. Macromol Mater Eng 2020;305(4).
[33] Victoria A, Edward Ries M, John Hine P. Use of interleaved films to enhance the properties of all-cellulose composites. Compos A Appl Sci Manuf 2022:107062.
[34] Hine, P.J. and M.E. Ries, *Composite Materials*. 2020: United Kingdom.
[35] Lee BCY, et al. A comprehensive review of Design of experiment (DOE) for water and wastewater treatment application - Key concepts, methodology and contextualized application. J Water Process Eng 2022;47.
[36] Mohammed A, et al. Alginate extraction from Sargassum seaweed in the Caribbean region: Optimization using response surface methodology. Carbohydr Polym 2020;245:116419.
[37] Montgomery DC. Design and analysis of experiments. New York: John Wiley & Sons; 2017.
[38] Vanaja K, Shobha Rani RH. Design of Experiments: Concept and Applications of Plackett Burman Design. Clin Res Regul Aff 2008;24(1):1–23.
[39] Owen MR, et al. Efficiency by design: optimisation in process research. Org Process Res Dev 2001;5(3):308–23.
[40] Weissman SA, Anderson NG. Design of Experiments (DoE) and Process Optimization. A Review of Recent Publications. Org Process Res Dev 2014;19(11):1605–33.
[41] Lee R. Statistical Design of Experiments for Screening and Optimization. Chem Ing Tech 2019;91(3):191–200.
[42] Sibanda W, Pretorius P. Comparative study of the application of central composite face-centred (CCF) and Box-Behnken designs (BBD) to study the effect of demographic characteristics on HIV risk in South Africa. Network Modeling Analysis in Health Informatics and Bioinformatics 2013;2(3):137–46.
[43] Victoria A, et al. Design of experiments in the optimization of all-cellulose composites. Cellul 2023;30(17):11013–39.
[44] Mwaikambo LY, Ansell MP. The determination of porosity and cellulose content of plant fibers by density methods. J Mater Sci Lett 2001;20(23):2095–6.

[45] Bawn, C.S.H., *Encyclopedia of polymer science and engineering*, H.M. JI Kroschwitz, N. Bikales, CG Overberger and G. Menges, Editor. 1985, John Wiley and Sons: New York.
[46] Pabari RM, Ramtoola Z. Application of face centred central composite design to optimise compression force and tablet diameter for the formulation of mechanically strong and fast disintegrating orodispersible tablets. Int J Pharm 2012;430(1–2):18–25.
[47] de Olveira LÁ, et al. Investigations on short coir fibre–reinforced composites via full factorial design. Polym Polym Compos 2018;26(7):391–9.
[48] Filho SLMR, et al. The impact behaviour of hybrid fibre-particle composites based on a full factorial design. Mater Today Commun 2022;31.
[49] Mohammed A, et al. Sargassum inspired, optimized calcium alginate bioplastic composites for food packaging. Food Hydrocoll 2023;135.
[50] Derringer G, Suich R. Simultaneous Optimization of Several Response Variables. J Qual Technol 1980;12(4):214–9.
[51] Adak B, Mukhopadhyay S. A comparative study on lyocell-fabric based all-cellulose composite laminates produced by different processes. Cellul 2016;24(2):835–49.
[52] Soykeabkaew N, Nishino T, Peijs T. All-cellulose composites of regenerated cellulose fibres by surface selective dissolution. Compos A Appl Sci Manuf 2009;40(4):321–8.
[53] Chen, J., *Chapter 4 - Synthetic Textile Fibers: Regenerated Cellulose Fibers*, in *Textiles and Fashion*, R. Sinclair, Editor. 2015, Woodhead Publishing. p. 79-95.
[54] Jiang X, et al. A review on raw materials, commercial production and properties of lyocell fiber. Journal of Bioresources and Bioproducts 2020;5(1):16–25.
[55] Sharma A, et al. Structure–property relations in regenerated cellulose fibers: comparison of fibers manufactured using viscose and lyocell processes. Cellul 2019;26(6):3655–69.
[56] Malheiro JMM, Salvado LRS. Microscopic study of bacteria-textile material interaction for hygienic purpose. Microsc Microanal 2009;15(S3):63–4.
[57] Anderson, M.J. and P.J. Whitcomb, *RSM simplified: optimizing processes using response surface methods for design of experiments*. 2016: Productivity press.
[58] Jankovic A, Chaudhary G, Goia F. Designing the design of experiments (DOE) – An investigation on the influence of different factorial designs on the characterization of complex systems. Energ Buildings 2021;250.
[59] Oliveira LÁ, et al. Evaluation of hybrid-short-coir-fibre-reinforced composites via full factorial design. Compos Struct 2018;202:313–23.